Cyclic loadings and crystallization of natural rubber: An explanation of fatigue crack propagation reinforcement under a positive loading ratio

Nicolas Saintier, Georges Cailletaud, Roland Piques

Cyclic loadings and crystallization of natural rubber: An explanation of fatigue crack propagation reinforcement under a positive loading ratio

N. Saintier [a,*], G. Cailletaud [b], R. Piques [b]

[a] LAMEFIP, Arts et Métiers ParisTech, Esplanade des Arts et Métiers, 33405 Talence Cedex, France
[b] Centre des matïeriaux P.M. FOURT, Ecole Nationale Supïerieure des Mines de Paris, UMR CNRS 7633, Evry Cedex 91003, France

Natural rubber is known to have excellent fatigue properties. Fatigue crack propagation studies show that, under uniaxial tension loading, fatigue crack growth resistance increases with the loading ratio, even if the peak stress increases. Studies dealing with crack initiation confirm this trend. If strain induced crystallization is believed to play a major role in this reinforcement process, it is not clear yet by which mechanism this reinforcement takes place. Using SEM investigation, it is shown here that the reinforcement process is associated with strong crack branching in the crack tip region. From experimental results it is shown that under particular reinforcing loading condition a cyclic strain hardening process can be observed on the natural rubber which is able to overcome classically observed softening effects. A cumulative strain induced crystallization process is proposed to explain the stress ratio effect on fatigue crack initiation and propagation properties of natural rubber.

Keywords:
Natural rubber
Fatigue
Crystallization
Crack branching

1. Introduction

Natural rubber's resistance to crack growth and its ability to withstand large strains without permanent deformation are two of the main reasons for its extensive use in many industrial applications. Most of them involve significant static and cyclic loading. The need for appropriate multiaxial fatigue life criteria has become crucial over the past 10 years. A good understanding of the micromechanisms involved in the fatigue crack initiation process are essential for the establishement of physically motivated criteria. In the case of natural rubber, in addition of damage mechanisms, specific reinforcing mechanisms still have to be understood. Indeed, under particular loading conditions (under uniaxial loading these particular conditions correspond to positive stress ratio tests), natural rubber shows an exceptional fatigue resistance so that damage mechanisms only cannot fully describe the fatigue behavior of natural rubber. A reinforcing mechanism must be taken into account in order to propose a fatigue life criterion suitable for all types of loading. The aim of this paper is not to propose such a criterion but rather to understand the origin of this mechanism so that a physically based criterion can be proposed (see [1,2] for a multiaxial fatigue life prediction method taking into account reinforcing mechanisms on natural rubber). The particular strength of natural rubber, as opposed to synthetic rubber on which such reinforcing mechanisms are not observed, has been attributed to its ability to crystallize upon stretching. Strain induced crystallization is believed to play a major role in fracture properties of rubber by inducing strong microstructural changes in the crack tip region. Strain induced crystallization of natural rubber has been largely investigated using numbers of techniques such as X-ray diffraction [3–6], infra-red spectrometry [7,8], birefringence [9], low-angle light scattering [10], Raman [11,12], or nuclear magnetic resonance [13,14]. These studies have resulted in a better understanding of the link between microstructural features (cross-link density, chemical composition, fillers, see [6] for more details), temperature and strain on natural rubber crystallization. The work of Trabelsi et al. [3], Siesler [7] and Toki et al. [4,5] give interesting results concerning the effect of cyclic deformation on strain induced crystallization, which is of prior importance when dealing with fatigue loading. However, the aim of these studies was not to link the strain induced crystallisation to the reinforcement processes observed under fatigue loading so that the loading frequencies were several orders of magnitude below the one usually encountered in fatigue tests, the type of strain cycles did not correspond to cases where reinforcement processes are observed, and finally the link with fatigue crack initiation mechanisms was not assessed. For these reasons no satisfactory answer to the reinforcement process observed under cyclic loading has yet been proposed.

In this paper we present the crack initiation mechanisms observed under reinforcing conditions and propose an explanation for the reinforcement under cyclic loading and its relation to strain induced crystallization.

* Corresponding author. Fax: +33 (0) 556845366.
E-mail address: nicolas.saintier@ensam.eu (N. Saintier).

2. Strain induced crystallization and fracture properties

Strain induced crystallization is due to the particular steric purity of the polyisoprenne backbone (in our case 99.9% polyisoprenne cis-1,4). By stretching, the conformational entropy decreases, which increases the ability of natural rubber to crystallize. Strain induced crystallization of natural rubber has been largely investigated using a number of techniques as stated in the previous section. The morphology of the strain/stress induced crystallization has been reported to have many different structures: fibrils, fibrils and folded lamellae, and shish-kebabs [15–18]. In all cases, the microstructure induced is strongly anisotropic. It exhibits strong covalent bonds in the direction of straining and weaker Van der Waals forces in the plane perpendicular to the straining direction.

Under simple tension, strain induced crystallization has been shown to be responsible for the upturn in modulus observed on the load–displacement curve for carbon-black filled natural rubber. The sensitivity of the strain induced crystallization rate to both the presence and type of fillers is high. Recently, Trabelsi et al. [19], Rault et al. [20] analysed strain induced crystallization by synchrotron X-ray diffraction and Chenal et al. [6] analysed the parameters governing strain induced crystallization in filled natural rubber giving a good understanding of the filler type effect. Since only one type of natural rubber was available for this study, it was not possible to analyze the filler type effect on the features related in this paper. At room temperature, where isotropic ("cold") crystallization is limited [21], failure properties of rubber are governed by strain induced crystallization. The anisotropic microstructure induced in the high-strain regions surrounding crack tips is believed to play a major role in fracture mechanisms by opposing a high strength structure in the direction of crack propagation [22]. Hamed and Kim [23] studied crack path under monotonic loading for both synthetic (cis-butadiene) and natural rubbers. For synthetic rubber, the direction of crack growth was found to be close to a path perpendicular to the loading direction. For natural rubber, cracks were found to deviate from this perpendicular direction so that final rupture was the result of successive crack initiation, propagation and deviation. The propensity to secondary cracking was found to depend on the initial crack length.

For fatigue loading, Cadwell [24] was one of the first to observe the reinforcement process under fatigue loading. He performed one-dimensional fatigue tests on natural rubber and styrene-butadiene rubber using dumbbell-like specimens. For styrene–butadiene rubber, at constant strain amplitude, increasing the mean stress was found to reduce the fatigue life. For natural rubber, the same tendency was observed for mean stress values lower than the stress amplitude. However, as soon as the mean stress was greater than the stress amplitude (corresponding to positive loading ratio tests), increasing the mean stress value was found to increase markedly the fatigue life. Lindley obtained similar results by investigating crack propagation rates under one-dimensional fatigue loading on pre-cracked specimens. He identified so-called "non-relaxing loading conditions" under which natural rubber exhibited enhanced crack growth resistance [25]. In the following sections "Non-relaxing conditions" will correspond to a type of loading where the load is never completely removed over a cycle (i.e., positive loading ratio tests). Conversely, relaxing conditions will correspond to loading cases where the load is fully relaxed during a cycle (i.e., loading ratio negative or null). It must be noticed that the reinforcement process was found to occur for the same loading conditions for un- and pre-cracked specimens. Using the tearing energy concept, Lindley proposed to compute the crack propagation rate as:

$$\frac{dc}{dn} = A_x(T_{max} - T_x) + r_z \quad (1)$$

Table 1
Composition of the natural rubber in parts by weight phr.

Rubber 100			
Zn oxide	10–20	Stearic acid	1
Carbon black N772	20	Carbon black N330	3
Sulfur	≥2	Plasticizers	5

where c is the crack length, n the number of cycles, T_{max} the maximum tearing energy, x the ratio T_{min}/T_{max}, T_x the dynamic crack growth limit, A_x the crack growth constant at the current x value, and r_z a material constant associated with the crack growth rate due to ozone attack.

However, in the case of cyclic loading, the process by which the crystallization enhances the fatigue life is not clear. Indeed, according to Eq. (1), during a cycle, the instant at which the maximum damage is reached corresponds to the instant of the maximum tearing energy (the crack propagation rate is controlled by the maximum tearing energy). However, since T_{max} corresponds to the maximum extension of the specimen, it must coincide with the maximum degree of crystallization at the crack tip. Then, how can one explain, from the micromechanism point of view, that reinforcement is controlled by both T_{min} and T_{max} (i.e., the loading ratio x), and not T_{max} only. Moreover, it should be noticed that if the x ratio is lower or equal to zero, whatever the maximum tearing energy, no reinforcement will be observed.

The following sections focus on experimental results which aim to propose an explanation of the reinforcement mechanisms under cyclic loading.

3. Experimental

3.1. Material

The elastomer used in the present study was a vulcanized natural rubber material filled with 23 parts of reinforcing carbon black (N772, N330) per hundred parts of rubber. Formulation and mechanical properties are given in Tables 1 and 2. Thin strips of material were cut from 150 mm × 150 mm × 2 mm rubber sheets. Those specimens were used for one-dimensional cyclic tensile tests presented in Section 4.2.3. Before testing, the material was preconditioned 100 cycles at the maximal elongation (in our case $\lambda = 3.5$) and at an elongation ratio $\lambda_{min}/\lambda_{max} = 0$ in order to limit stress softening (Mullins effect) during cyclic loading. Using this procedure the material behavior was stable during cyclic loading at $\lambda = 3.5$ but could still show some stress softening at larger elongation values as it is usually the case with Mullins effect. The value of $\lambda_{max} = 3.5$ was considered as a good compromise giving sufficient Mullins effect vanishing and low fatigue damage.

3.2. Fatigue testing

Fatigue testing was carried out on axisymmetrical diabolo-shaped specimens (see Fig. 1) molded by injection, almost uniaxial when carrying out push-pull testing. The elastomer was bonded to the metal end pieces during the vulcanization process. Fatigue testing was carried out under displacement control using electro-mechanical fatigue machines developed at the laboratory. Specimen compliance was much greater than that of the

Table 2
Room temperature mechanical properties.

Density (g/m^3)	A shore hardness	UTS (MPa)	ε_{fail} (%)	300% elong. modulus (MPa)
1.1	48	25.3	500	7.8

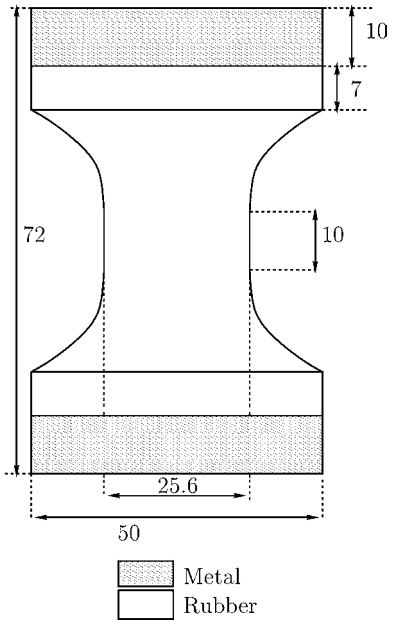

Fig. 1. Specimen geometry used for fatigue tests (dimensions in mm).

fatigue machine. Hence, the applied displacement was considered as being fully applied to the specimen. Fatigue machines were supplied with waveforms generated by a digital-to-analogue converter under PC control. Cycles, load and displacement data were recorded by the PC via an analogue-to-digital converter. All tests were carried out at room temperature and at low frequency (1.5 Hz) due to the large displacements involved when testing elastomers. At that frequency, the temperature of the specimen was found to be stable during fatigue tests. Fatigue tests were conducted at least to crack initiation, and in most cases to rupture. The number of cycles to crack initiation N_i is conventionally defined as the number of cycles necessary to obtain a crack of a 1 mm size. The parameter N_i is difficult to determine unambiguously since neither compliance changes nor potential drop technique can be used with those materials. Hence, the specimen surface was observed using an optical microscope and N_i obtained by visual inspection and measurement. In this paper, only the one-dimensional database obtained from push–pull fatigue tests on diabolo specimens (positive and negative loading ratios) will be presented. Multiaxial fatigue tests results and modeling can be found in [26,1].

3.3. SEM observations and specimen preparation

Specimen surfaces were observed after fatigue testing using a field effect Zeiss scanning electron microscope (SEM). Microtensile specimens were cut at the diabolos' surface and observed under tension in the SEM chamber using a Deben tensile testing stage. The typical shape of the microtensile specimens were strips of 50 mm × 15 mm × 5 mm. Areas observed by SEM were located in the center of the microtensile specimens. The elongation applied for SEM observation was not greater than 10% of the maximum elongation reached during the fatigue testing.

3.4. RX diffraction measurements

Three techniques were used: Laue diffraction (anti cathode Mn, voltage 40 kV, current 30 mA), pole figures (anti cathode Cr, voltage 40 kV, intensity 40 mA), and wide angle X-ray diffraction (anti cathode Cu, voltage 40 kV, intensity 30 mA). Pole figures were performed at the LIMM (Arts et Métiers ParisTech) laboratory, using a 3-axis SIEMENS D500. Wide angle X-ray diffraction spectrography (WAXS) was performed at the laboratory using a 1-axis SIEMENS D500 equiped with a proportional linear ELPHYSE detector. Measurements were conducted while straining the specimen at different strain levels ranging from 0% to 450%. WAXS scans were de-convoluted to extract the contribution of the crystalline structure from the rest of the material. The degree of apparent crystallization was calculated using the assumption made by many authors [27–30,22], which is that at a given strain level λ the total diffracted intensity can be partitioned into an amorphous and a crystalline phase contribution such as:

$$I^{\lambda}_{\text{total}} = I^{\lambda}_{\text{amorphous}} + I^{\lambda}_{\text{crystalline}} \tag{2}$$

If the total diffracted intensity is assumed constant (the number of diffracting items is constant, only their arrangement is modified), a crystallinity index X_c can be defined as:

$$X_c = 1 - \frac{I^{\lambda}_{\text{amorphous}}}{I^{0}_{\text{total}}} \tag{3}$$

In this paper, X_c will only be considered as a crystallization index and not the absolute value of crystallized chains. Indeed, the measurement of I_{amorphus} (see Eq. (3)) by WAXS scans supposes to have a non-oriented amorphous phase (one assumes that the diffracted intensity associated with the amorphous halo is independent of the direction of the scan with respect to the tensile direction), which is not really the case for natural rubber under tension. Each WAXS scan was deconvoluted so that the area of each peak (amorphous + crystalline peaks) could be computed and X_c achieved. A Pearson VII type function was chosen for describing the diffraction peak shape:

$$I(x) = \frac{I_0}{1 + 4(2^{1/m} - 1)((x - x_0)/\Delta\phi)}$$

where I_0 is the peak height, m a shape parameter, x_0 the peak position, $\Delta\phi$ the half height width. A typical deconvoluted scan is given in Fig. 2.

4. Results and discussion

4.1. Uniaxial fatigue results

One-dimensional fatigue results have been reported in Fig. 3(a) in a Haigh diagram with two parameters, the stress amplitude and mean stress. The dashed lines represent optimized iso-contour lines using a simple bi-linear model. It is interesting to note that the fatigue life sensitivity to the loading ratio R is in agreement with that observed by Cadwell in his early studies. At constant stress

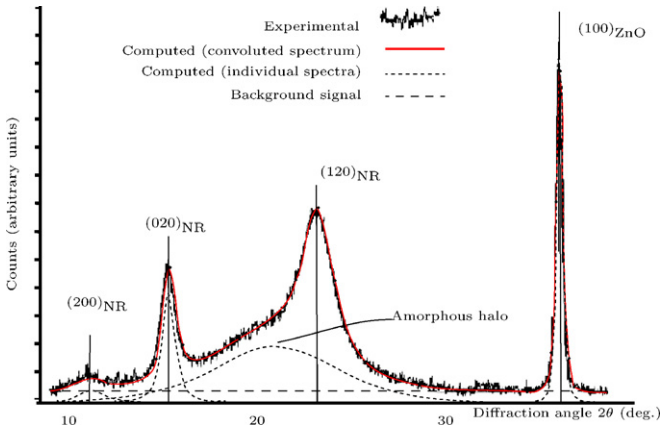

Fig. 2. Computed and experimental diffraction spectrum for an elongation of λ = 4.

amplitude, increasing the mean stress increases the fatigue life for positive loading ratio tests. This phenomenon is characteristic of natural rubber and shows the reinforcement at positive loading ratios under one-dimensional loading. Taking into account the reinforcement process in the fatigue life modeling makes it possible to unify the experimental results for relaxing and non-relaxing conditions as shown in Fig. 3(b). More details on the fatigue modeling and discussions on the validity of such a representation can be found in [1,36]. The following section focuses on the very first stage of crack propagation where the crack size is very close to the size of the flaw from which it initiates.

4.2. SEM observations

4.2.1. Cracks at initiation

The very first stage of fatigue damage initiation on the material of the study has been closely investigated and was reported in [2]. Fig. 4(a) represents a crack at initiation (observed under tension) after fatigue testing under relaxing conditions. In this particular case, the crack initiated on a carbon black agglomerate of about 100 μm (see Fig. 4(b)). The large crack blunting is characteristic of an elastomeric material. At the crack tip, small fibrils can be observed (see Fig. 4(c)) which confirm that the crack has been initiated and is propagating at this stage. The crack is semi-elliptical in a plane perpendicular to the tensile direction. Despite strong crack blunting, fibrils are only present in a narrow and continuous band at the crack tip. From those observations we can conclude that the crack propagates on a single plane under these particular conditions (no crack deviation at this stage of the crack propagation process). Fig. 5 shows a crack initiation for non-relaxing conditions. The crack morphology for relaxing and non-relaxing conditions are obviously different. Strong multi-cracking and crack deviation can be observed under non-relaxing conditions. In this particular case, not less than 7 different crack tips can be identified with typical crack length of 100 μm. Moreover, at larger magnification, those microcracks appear to present additional secondary cracking with characteristic secondary crack length in the 2–10 μm range. Below 2 μm, micro-cracks can hardly be identified or considered as cracks.

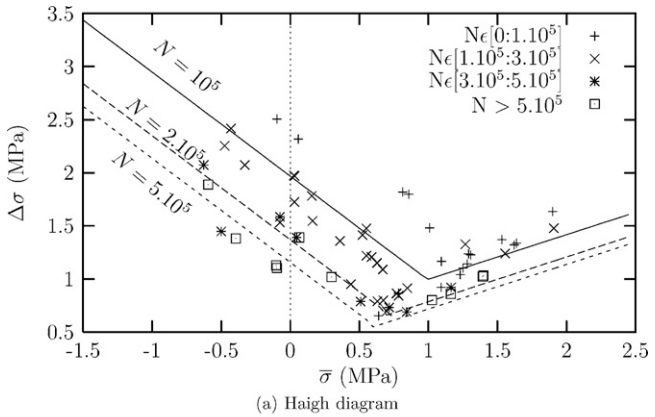

(a) Haigh diagram

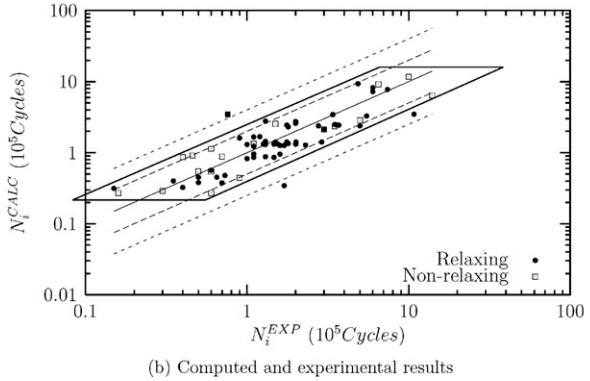

(b) Computed and experimental results

Fig. 3. Uniaxial fatigue test results and comparison with predicted results. (a) Haigh diagram. (b) Computed and experimental results.

4.2.2. Meso cracks

It has been shown in [2] that fatigue life is mostly controlled by a crack propagation process. The incubation time for a crack to be generated from a flaw (i.e., an inclusion for example) represents only 10–20% of the total fatigue life. In order to observe fatigue cracks morphologies on 1–2 mm cracks, interrupted fatigue tests were performed. The plane of observation was chosen so that it was perpendicular to the crack plane and to the crack front (see Fig. 6). To ensure a perfect sectioning while not inducing any damage during the preparation of the specimen, a cryogenic microtome was used (at sectioning temperature $T = 90\,^{\circ}C$). As observed on microcracks, the crack morphology of macrocracks obtained under relaxing and non-relaxing conditions are very different as shown in Fig. 7. Under relaxing conditions (Fig. 7(a)), the crack path is very close to a path perpendicular to the loading direction. For non-relaxing, strong crack branching is observed. Observations at higher magnifications show that the secondary cracking observed in Fig. 7(b) is accompanied by smaller scale secondary cracking in a fractal way. Then, the crack propagation process is not the result of a single crack front motion but of multiple crack fronts propagating simultaneously. This provides a first explanation of the fatigue life reinforcement or the crack propagation resistance increase for non-relaxing conditions: by enabling strong secondary crack formation, those particular loading conditions allow the dissipation of much more energy than it would in a single crack propagation process (i.e., under relaxing conditions) and thus significantly reduce the global crack growth rate. It is interesting to note that the degree of branching increases with the crack length. This confirms previous observations made by Hamed et al. [31] under monotonic loading. However, the extent of secondary cracking in the present case is much larger than that observed by Hamed et al. Moreover, in our case, despite secondary cracking, the global crack propagation direction stays perpendicular to the applied loading direction, at least for crack sizes up to a few millimeters in size.

Using the tearing energy concept proposed by Lindley, there is a competition between the damage process controlled by the maximum tearing energy and a reinforcement process which induces the secondary cracking. However, the question of what induces this secondary cracking, and thus which mechanical parameter controls the reinforcement, is still open.

4.2.3. Crack branching and strain induced crystallization

Crack branching is a well known phenomenon in fracture mechanics. It can be due to the type of loading (high speed crack propagation, for example) or to some sort of anisotropy induced by the material (micro)structure (composite material, for example). Since one-dimensional fatigue loading has no natural propensity for inducing crack branching, the origin of crack branching must be found in the material itself. By comparing natural rubber behavior to that of synthetic rubbers, strain induced crystallization is most likely to play a major role in this process by creating a highly heterogeneous and anisotropic zone at the crack tip.

Under uniaxial tension, crystallization was found to start at about 150% strain (see Fig. 8). The maximum degree of crystallization of 25% was reached at approximatively 400% strain. The sharp reflections obtained on the X-ray diffraction patterns and associated pole figures have shown a well-developed three-dimensional structure, with the chain axis being along the tensile direction. Moreover, there is a rotational symmetry around the chain axis.

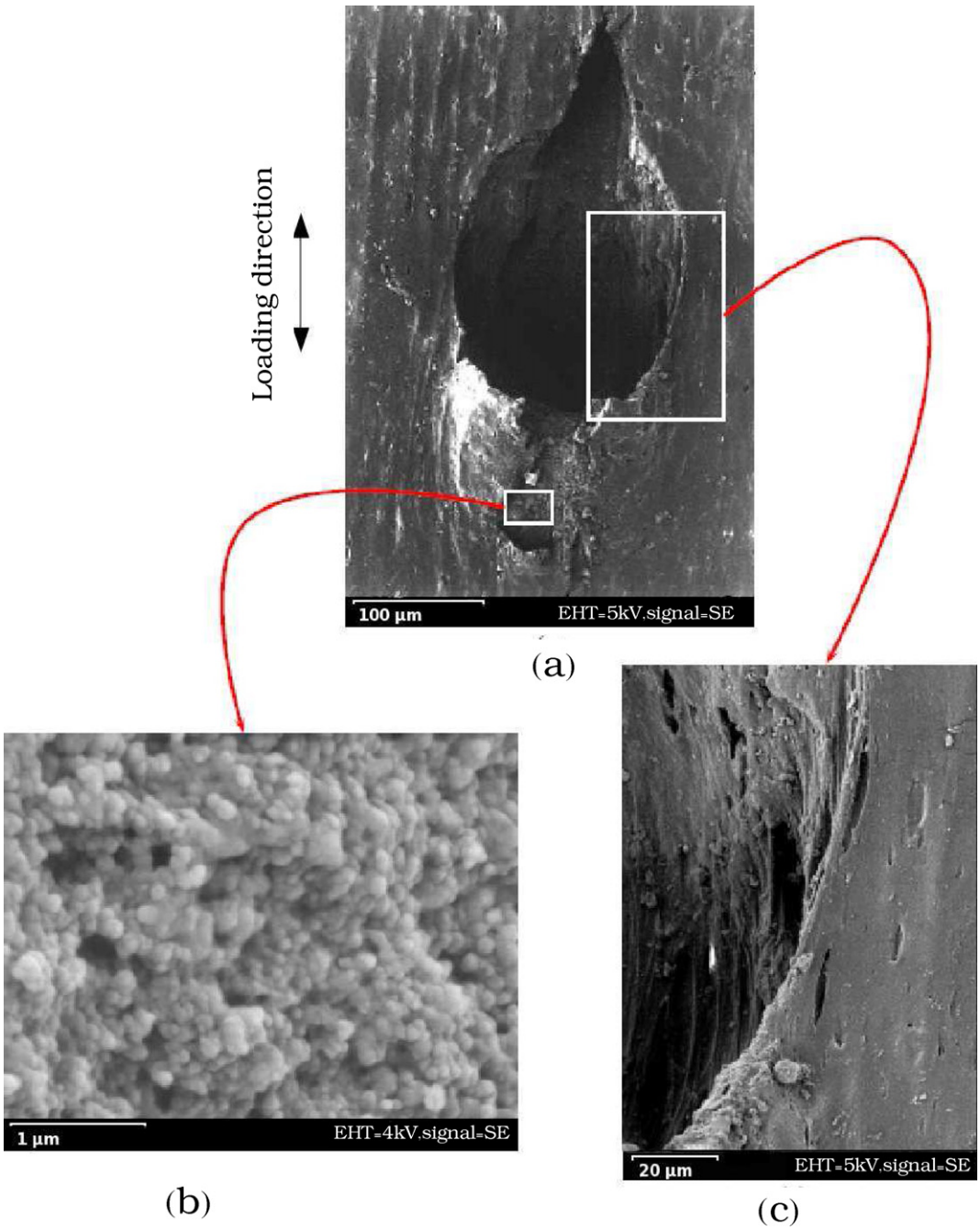

Fig. 4. SEM image of a crack initiation under relaxing conditions on a diabolo specimen (loading ratio $R = -0.3$).

These results are in accordance with already published results [32,4,33].

The sequential measurement procedure used makes it possible to characterize the induced microstructure. However, since WAXS diffractometer scans take at least 45 min to complete, no information could be obtained to characterize the dynamic behavior of strain induced crystallization and the effect of cyclic loading.

Toki [4] equiped a WAXS diffractometer with a special device which could stretch the sample at constant speed (55 mm/min). They followed the diffracted intensity of a unique peak (1 2 0) as function of the applied strain. They found that crystallites formation (loading) and fusion (un-loading) follow different kinetics, so that over a cycle, at a given elongation the degree of crystallinity is higher during un-loading than it is during loading. Further work of Toki [33] and Rault et al. [20] using in situ synchrotron X-ray, have shown similar results. However, they investigated the evolution of crystallinity over only one cycle and the effect of both non-relaxing conditions and several cycles has not been established. Moreover, the loading frequencies used in those studies were far from the one investigated here (10^{-4} Hz for Rault et al. [20] versus 1 Hz in this study). Since it was not possible for us to equip our diffractometer with such a device, and that the measurement of crystallization dynamic at high strain rates is a challenge in itself, another parameter was used as a tracer of crystallinity: the global mechanical response. Indeed, since the upturn in modulus corresponds to the start of crystallization [4,33] (this point is still quite largely discussed in the literature since some authors have shown that crystallization might start earlier [3] but all agree that the upturn represents at least an upper bound for the minimum strain necessary for the crystallization to start), the evolution of the

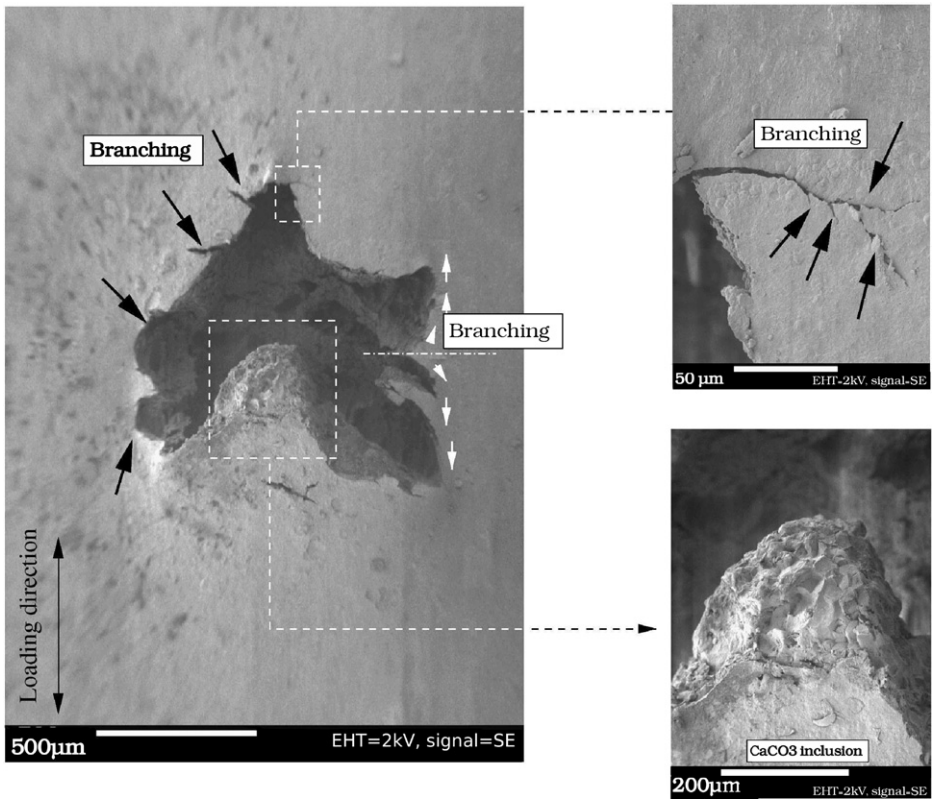

Fig. 5. SEM image of a crack initiation under non-relaxing conditions on a diabolo specimen (loading ratio $R = 3.8$).

stress–strain response at high strains should give good information on the crystallinity evolution. More precisely, if the crystallization affects the local tangent modulus, any modification in the dynamic of strain induced crystallization (for example due to the type of loading applied) should produce an increase in the level of stress reached at a given elongation. Strain controlled cyclic tensile tests were performed with both relaxing and non-relaxing conditions. The maximum strain applied was chosen constant for both conditions ($\lambda_{max} = 4.75$). For non-relaxing conditions the minimum strain applied was changed at each cycle to increasing values ranging from $\lambda_{min} = 1.5$ to $\lambda_{max} = 4$. In this section, the term cycle will refer to a successive loading and unloading sequence. The applied strain path is given in Fig. 9(a). In order to clearly identify any stress softening or hardening effects the nondimensional quantity γ_n is computed as follows:

$$\gamma_n = \frac{\sigma_{max,n}}{\sigma_{max,1}} \tag{4}$$

where $\sigma_{max,1}$ (resp. $\sigma_{max,n}$) is the maximum stress reached during the first (resp. nth) cycle. Results are given in Fig. 9(b) and 10. Under relaxing conditions, the maximum stress slowly decreases at each cycle. This phenomenon is classically observed for rubbers and is known as the Mullins effect which can still take place (with far less intensity) despite the pre-stabilization. Under non-relaxing conditions, the maximum stress first decreases (stage 1), following the relaxing condition response, but then increases markedly as soon as the minimum strain reaches 75% (stage 2). The stress increase can be seen as a cyclic hardening or reinforcement of the material under these particular loading conditions. This reinforcement is able to overcome the softening effect (Mullins effect) since the maximum stress reached under non-relaxing conditions at the 7th cycle is 12% greater than the one reached at the very first cycle and 25% greater than the one reached under relaxing conditions. This result gives further understanding of the reinforcement mechanisms observed under fatigue testing under non-relaxing conditions and, to the authors' knowledge, has never been reported in the literature. This cyclic hardening can be understood as the result of a cumulative effect of crystallization under non-relaxing conditions. Indeed, if crystallization is not completely annealed at each cycle, every successive loading will induce a new increase in the crystallinity level until saturation is reached as shown by the evolution of $\Delta\sigma_{max}$. This effect is also the consequence of the time dependance of strain induced crystallization: due to the cyclic nature of the loading, crystallization is not fully achieved during cyclic loading. However, it is still difficult to correlate the stress and crystallinity kinetics in a quantitative way (such a work implies real scientific challenges:

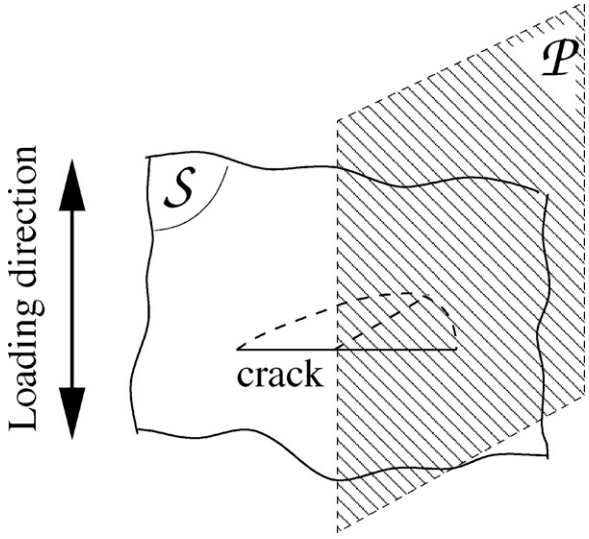

Fig. 6. Relative position of the specimen surface S and the plane of observation P.

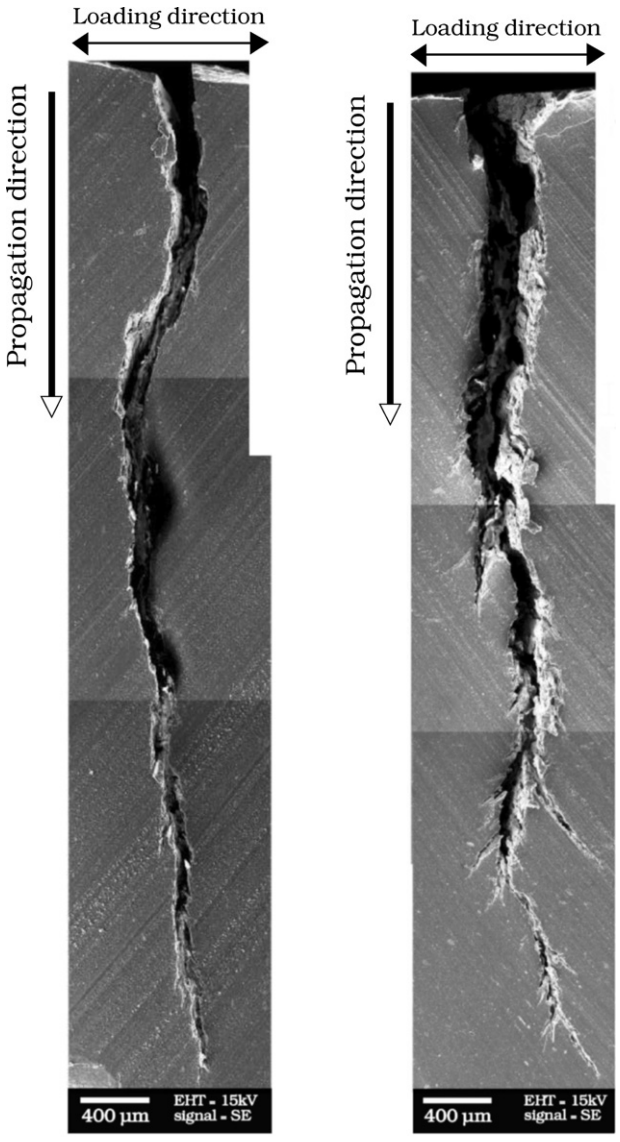

(a) Relaxing conditions (loading ratio R=-0.3)

(b) Non-relaxing conditions (loading ratio R=4.2)

Fig. 7. Crack path under relaxing and non-relaxing conditions in a plane perpendicular to the crack propagation plane [31]. (a) Relaxing conditions (loading ratio $R = -0.3$). (b) Non-relaxing conditions (loading ratio $R = 4.2$).

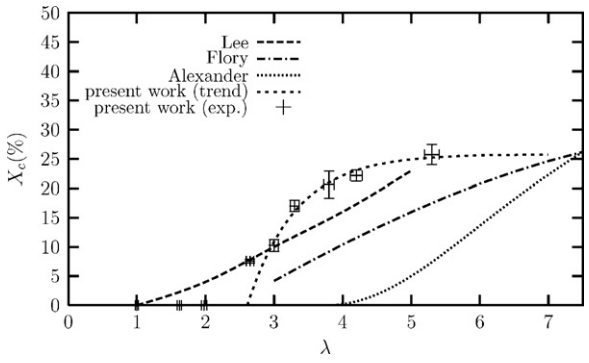

Fig. 8. Evolution of the crystallinity index as a function of applied elongation. Comparison with previously published results by Lee and Donovan [22], Alexander [34], Goppel [35] and Flory [15].

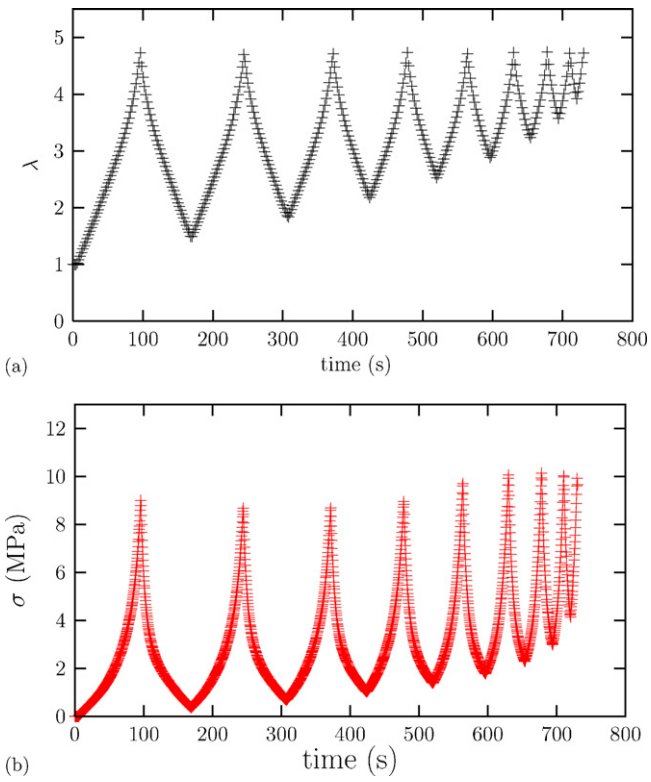

Fig. 9. Applied elongation path and Cauchy Stress response.

experimentally, crystallinity kinetics under dynamic loading have to be studied using synchrotron-WAXS and numerically, constitutive laws including strain induced phase transformation still have to be developed for those materials). After Toki [4], the evolution of the X-ray scattering intensity (i.e., apparent crystallization) under relaxing conditions is given in Fig. 11(a). Using those results we propose the evolution of the apparent crystallization for non-relaxing conditions as shown in Fig. 11(b). When the minimum strain is kept below a threshold value there is no cumulative effect. It should be noted that this threshold value is much lower than the strain needed to first crystallize. It is effectively observed on the stress response with a strain threshold around 75% whereas a 150% strain elongation is needed to first crystallize the natural rubber. Once the threshold is overcome, the cumulative effect can take place and cyclic hardening occurs. Stage 3 corresponds to the stabilization of the reinforcement process which is progressively overcome by stress relaxation mechanisms taking place at such high strain levels.

The strain rate effect observed in Fig. 10 can be explained by considering that since the crystallization takes time to settle, the higher the frequency, the lower the degree of crystallinity at the end of the test (at least using the particular strain path proposed here). The reinforcement should then be less pronounced for higher frequencies (higher strain rates). This trend has been observed on the presented experimental results.

5. Cumulative effect and crack branching

The aim here is to better understand from the previous results the microstructural evolution in the crack tip loading under relaxing and non-relaxing conditions. Under relaxing conditions the evolution of crystallinity follows the experimental results obtained by Toki [4] and can be modeled as shown in Fig. 11(a). At each cycle the crack tip is fully unloaded so that strain induced crystallization disappears and the crystallinity level restarts from zero.

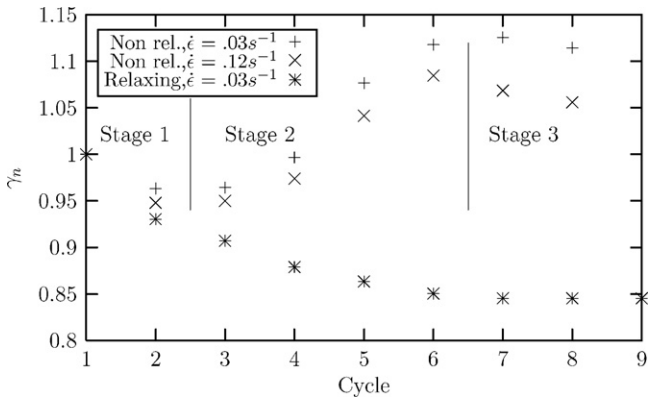

Fig. 10. Stress hardening for two different strain rates compared to the natural rubber behavior under relaxing conditions.

Under non-relaxing conditions, it is believed that a cumulative process takes place. The crystallinity in the crack tip region progressively increases until saturation, following the process proposed in Fig. 11(b). The degree and size of the crystallization zone at the crack tip is much larger than the ones reached under relaxing conditions. However, it has not been experimentally possible to fully demonstrate it by direct crystallinity measurement during this study. It should be noted that in order to demonstrate this cumulative process not only must the diffraction measurements be done at the same time as the deformation process but at loading frequencies sufficiently high to show this effect. The integration time of the measurement method must be compatible with the loading frequencies (a few Hz).

From the crack propagation process point of view, strong anisotropic microstructure takes place ahead of the crack tip when the cumulative process of crystallization takes place. In that case, the crack propagates continuously in an anisotropic media which results in symmetry being lost in the crack tip region and consequently the crack branching observed experimentally. This is illustrated in Fig. 12. Under uniaxial loading and relaxing conditions (Fig. 12(a)) the fatigue crack propagates normally to the loading direction and without strong deviation due to the weak anisotropy induced in the crack tip region. On the contrary, under uniaxial loading and non-relaxing conditions (Fig. 12(b)) the anisotropy caused by strain induced crystallization and the cumulative process (crystallites are symbolized by short vertical segments) makes

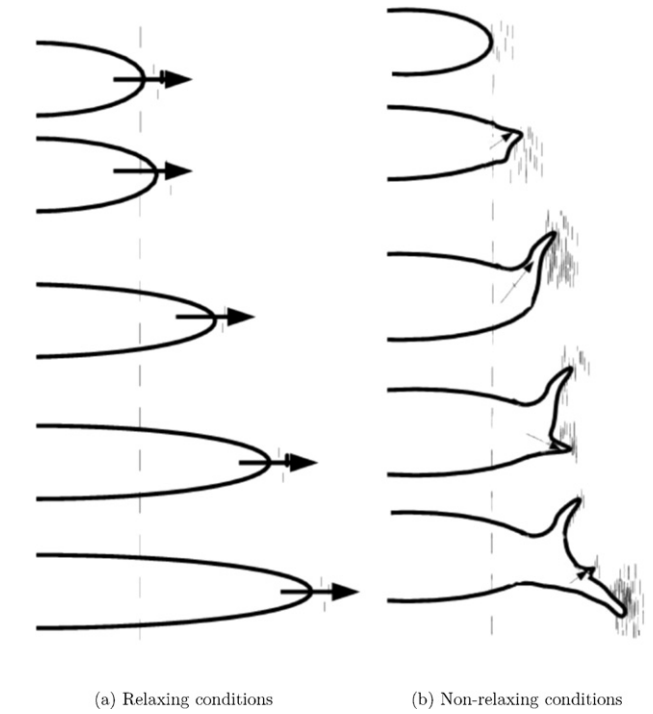

Fig. 12. Crack propagation process for relaxing and non-relaxing conditions (multiple crack branching obtained by repetition of this elementary sequence at the different scales). (a) Relaxing conditions. (b) Non-relaxing conditions.

the crack to deviate from the natural crack propagation direction. At any new crack tip formed, the process takes place again so that strong crack branching is observed as illustrated. Moreover, because the crack deviation process takes place at different scales simultaneously we obtain the fractal-like crack branching patterns observed. The proposed cumulative process confirms that when considering crack propagation modeling, both minimum and maximum tearing energies must be considered as proposed by Lindley [25]. However, from our observations it is believed that the cumulative process (reinforcement process) may influence not only the crack propagation threshold T_x but would play a role throughout the propagation process.

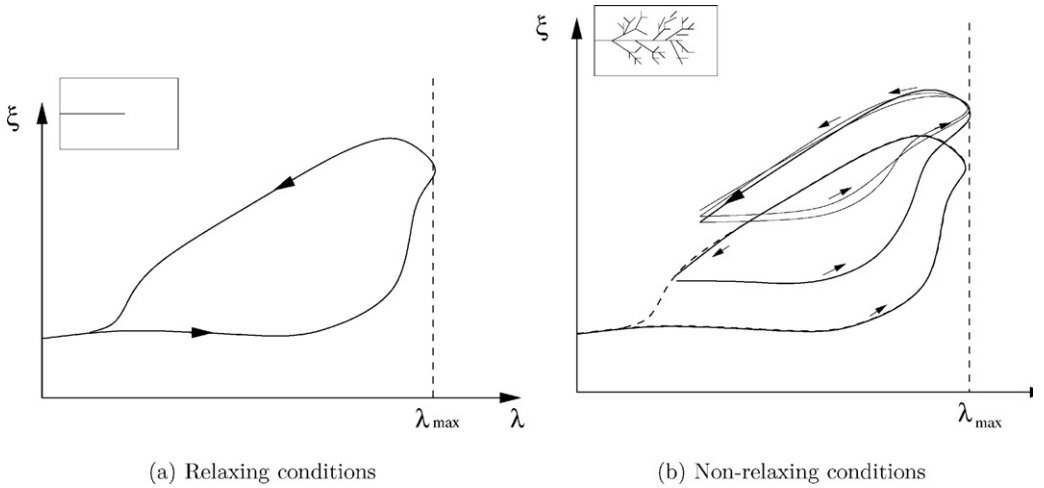

Fig. 11. Crystallinity evolution under relaxing conditions adapted from Toki et al. [4] and proposed evolution under non-relaxing conditions. (a) Relaxing conditions. (b) Non-relaxing conditions.

6. Conclusions

Using SEM observations it was shown that the excellent fatigue resistance properties under non-relaxing conditions are related to strong crack branching extending in a fractal-like behavior during both the initiation and the propagation process. The crystallization process was studied using WAX diffraction. A cyclic hardening has been observed on a natural rubber using non-conventional stress–strain paths. This cyclic hardening was understood as the result of a cumulative process of strain-induced crystallization which progressively hardens the material. Toki's results on crystallization kinetics under relaxing conditions have been used to propose crystallization kinetics under non-relaxing conditions which explain the minimum tearing energy influence on crack propagation rates observed by Lindley et al. Further experimental and numerical work in that field are clearly needed. In particular, in situ synchrotron-WAXS during cyclic loading would be of great interest to better characterize the crystallization kinetics under cyclic loading. Also, constitutive laws taking into account time dependent strain induced phase transformation are needed in order to better assess the relationship between the strain level and the crystallinity level. Finally, comparisons with materials having different crystallization kinetics (modifying the filler type or using crystallizable synthetics rubbers) are needed.

References

[1] N. Saintier, G. Cailletaud, R. Piques, Int. J. Fatigue 28 (2006) 530–539.
[2] N. Saintier, G. Cailletaud, R. Piques, Int. J. Fatigue 28 (2006) 61–72.
[3] S. Trabelsi, P.A. Albouy, J. Rault, Macromolecules 35 (2002) 10054–10061.
[4] S. Toki, T. Fujimaki, M. Okuyama, Polymer 41 (2000) 5423–5429.
[5] S. Toki, I. Sics, S. Ran, L. Liu, B. Hsiao, S. Murakami, K. Senoo, S. Kohjiya, Macromolecules 35 (2002) 6578–6584.
[6] J.-M. Chenal, C. Gauthier, L. Chazeau, L. Guy, Y. Bomal, Polymer 48 (2007) 6893–6901.
[7] H. Siesler, Appl. Spectrosc. 39 (1985) 761–765.
[8] H. Siesler, Macromol. Chem. Macromol. Symp. 5 (1986) 151–167.
[9] P. Mott, C. Roland, Macromolecules 29 (1996) 6941–6945.
[10] W. Yau, R. Stein, J. Polym. Sci. A26 (1968) 1–30.
[11] C. Jones, Spectrochim. Acta A 47 (1991) 1313–1319.
[12] A. Healey, P. Hendra, Y. West, Polymer 37 (1996) 4009–4024.
[13] F. Larsen, T. Rasmussen, W. Pedersen, N. Nielsen, H. Jakobsen, Polymer 40 (1999) 7013–7017.
[14] S. Oh, J. Koenig, J. Polym. Sci. B 38 (2000) 1417–1423.
[15] P. Flory, J. Chem. Phys. 15 (1947) 397–401.
[16] R. Smith, A. Black, Rubber Chem. Technol. 37 (1964) 338.
[17] E. Andrews, Proc. R. Soc. A 270 (1962) 232–241.
[18] E. Andrews, Proc. R. Soc. A 273 (1964) 562–584.
[19] S. Trabelsi, P.A. Albouy, J. Rault, Macromolecules 36 (2003) 9093–9099.
[20] J. Rault, J. Marchal, P. Judeinstein, P.A. Albouy, Macromolecules 39 (2006) 8356–8368.
[21] I. Choi, C. Roland, Rubber Chem. Technol. 70 (1997) 202–210.
[22] D. Lee, J. Dononvan, Rubber Chem. Technol. 60 (1987) 910–924.
[23] G. Hamed, H. Kim, Rubber Chem. Technol. 72 (1999) 895–910.
[24] S.M. Cadwell, R.A. Merrill, C.M. Sloman, F.L. Yost, Ind. Eng. Chem. 12 (1940) 19–23.
[25] P.B. Lindley, Int. J. Fract. 9 (1973) 449–462.
[26] N. Saintier, Ph.D. dissertation, Ecole des Mines de Paris (2001).
[27] M. Cyr, B. Husson, A. Carles-Gibergues, J. Phys. IV 8 (1998) 5–23.
[28] J. Sahores, Adv. X-Ray Anal. 16 (1973) 186–197.
[29] A. Wims, M. Myers, J. Johnson, C.J.M., Adv. X-Ray Anal. 29 (1995) 281–290.
[30] D. Johnson, Adv. X-Ray Anal. 24 (1981) 25–36.
[31] G. Hamed, H. Kim, A. Gent, Rubber Chem. Technol. 69 (1996) 807–818.
[32] J. Maghill, Rubber Chem. Technol. 68 (1995) 507–539.
[33] S. Toki, I. Sics, S. Ran, L. Lizhi, Rubber Chem. Technol. 77 (2004) 317–335.
[34] L. Alexander, S. Ohlberg, G. Russell-Taylor, J. Appl. Polym. Sci. 26 (1955) 1068–1075.
[35] J. Goppel, J. Arlman, Appl. Sci. Res. A1 (1949) 462–474.
[36] A. Andriyana, N. Saintier, E. Verron, Int. J. Fatigue 32 (2010) 1627–1638.